Embedded-atom method study of the effect of the order degree on the lattice parameters of Cu-based shape memory alloys

1994 J. Phys.: Condens. Matter 6 4601

(http://iopscience.iop.org/0953-8984/6/24/019)

J. Phys.: Condens. Matter 6 (1994) 4601–4614. Printed in the UK

Embedded-atom method study of the effect of the order degree on the lattice parameters of Cu-based shape memory alloys

Jianian Gui, Yanling Cui†, Shengqiu Xu, Qinglin Wang, Yiying Ye, Meizhi Xiang and Renhui Wang

Department of Physics, Wuhan University, 430072 Wuhan, People's Republic of China

Received 11 October 1993, in final form 9 February 1994

Abstract. Using the embedded-atom method, the variation in the total energies and lattice parameters with the degree of long-range order has been calculated for the parent and $18R_1$ martensite phases for several Cu–Zn–Al and Cu–Al–Ni shape memory alloys. It was found that the bond angle φ, i.e. the angle between lines connecting the nearest neighbours in the basal plane of the martensite, increases with increase in degree S_{B2} of B2-type order for both Cu–Zn–Al and Cu–Al–Ni alloys. When the degree S_{L2} of $L2_1$-type order increases, the bond angle φ increases for the Cu–Zn–Al shape memory alloys, but it decreases for the Cu–Al–Ni shape memory alloys. This result agrees well with experiment.

1. Introduction

Compared with Ti–Ni-based shape memory materials (SMMs) which are the most popular SMMs on the market, Cu-based SMMs have the advantage of a lower price. Since the structures of the Cu-based SMMs are closely related to the shape memory effect, thermoelastic behaviour and other characteristics, much effort has been made to study their structures and structure changes during heat treatment and thermal cycles both experimentally and theoretically.

Delaey and his colleagues (Delaey 1967, Delaey *et al* 1981) studied the splitting of some x-ray diffraction line pairs, such as $(\bar{1}22)$–(202), $(1\,2\,10)$–$(\bar{2}\,0\,10)$ and (040)–(320) pairs of $18R_1$ martensite. They defined a splitting parameter $\rho = \sin^2\theta_{202} - \sin^2\theta_{\bar{1}22}$ with θ_{hkl} being the Bragg angles of the (hkl) reflections. The splitting parameter increases with increasing deviation from the regular hexagonal arrangement of the atoms on the basal plane, which depends in turn on the type and degree of the long-range order, the composition of the alloy and the relative sizes of the constituent atoms. On the basis of the hard-sphere model, Tadaki *et al* (1975) pointed out that the ordering distorts the exact hexagonal configuration of atoms on the basal plane which leads to the formation of the modified martensitic structures, such as M9R and $M18R_1$, instead of the normal martensites (N9R and $N18R_1$). Delaey *et al* (1981) supposed that the $B2$-type ordering is liable to produce more severe deviation from the regular hexagonal configuration than the A2-type disordering and $D0_3$-type ordering do.

The importance of the atom configuration in the basal plane of the martensites in Cu–Zn–Al shape memory alloys lies in that it relates to the temperature M_s (Ahlers 1974, Delaey

† Also at Department of Fundamental Courses, Jiaozuo Mining Institute, 454159 Henan Province, People's Republic of China.

0953-8984/94/244601+14$19.50

et al 1981) and martensite stabilization during aging (Scarsbrook *et al* 1982, Delaey *et al* 1984). Recently Gui *et al* (1990) introduced a bond angle φ in the basal plane, i.e. the angle between lines connecting the nearest neighbours in the basal plane of the $18R_1$ martensite, which is a more general parameter for describing the atom configuration in the basal plane than the splitting parameter ρ is. The value $\varphi = 60°$ corresponds to the regular hexagonal arrangement of atoms in the basal plane. In this case the $(\bar{1}22)$ lattice plane distance $d_{\bar{1}22}$ and the (202) lattice plane distance d_{202} are the same; hence the corresponding line-pair splitting parameter $\rho = \sin^2\theta_{202} - \sin^2\theta_{\bar{1}22} = 0$. With increase in the bond angle φ, the difference between $d_{\bar{1}22}$ and d_{202} increases and consequently the splitting parameter ρ increases. The splitting parameters ρ for other line pairs, such as $(1\,2\,\bar{1}0)$–$(\bar{2}\,0\,10)$ and (040)–(320), behave similarly. They found that the directly quenched Cu–Zn–Al $M18R_1$ martensite changes its lattice parameters towards those of the $N18R_1$ martensite during aging, in accordance with the results observed by Scarsbrook *et al* (1982) and Delaey *et al* (1984) while the degree of long-range order does not change substantially during martensite aging. The lattice parameters of step-quenched $M18R_1$ martensite remain invariant during aging. On the basis of the lattice parameter change during martensite stabilization, Delaey *et al* (1984) and Gui *et al* (1990) considered a possible mechanism of the martensite stabilization, i.e. the deviation from the invariant plane condition.

Since the hard-sphere model applied by Ahlers (1974), Tadaki *et al* (1975) and Delaey *et al* (1981) to the study of the martensite structure is only a rough approximation, it would be very interesting to study the martensite structure by means of more accurate atomistic simulation. Although the first-principles methods are the most rigorous, they are limited to very small systems and need a large computer with a higher speed. As a new semi-empirical method of calculating the ground-state properties of realistic atom systems, Daw and Baskes (1984) developed the embedded-atom method (EAM) based on density-functional theory. The EAM has then been further extended and modified so that a large number of elements, including the elements with FCC, BCC, HCP and diamond structure types, can be treated and so that it can be applied to a wide range of problems (see Foiles *et al* (1986), Oh and Johnson (1988), Baskes *et al* (1989), Adams and Foiles (1990), Chen *et al* (1990), Baskes (1992), and references therein). Other empirical methods, e.g. the method developed by Finnis and Sinclair (1984) which is based on the second-moment approximation to the tight-binding method, and the methods developed by Ercolessi *et al* (1986) and by Smith and Banerjea (1987), are all equivalent to the EAM mathematically. The EAM has been widely used at Wuhan University to study a variety of problems, including surface relaxation (Ning *et al* 1988), a stability comparison of several icosahedral structure units of Al–Cr alloys (Liu *et al* 1991) and the stability of the Al–Li–Cu icosahedral quasicrystal (Nie *et al* 1993).

In the present paper we calculate the variation in the total energies and lattice parameters with the degree of long-range order for the parent and 9R and $18R_1$ martensite phases in several Cu–Zn–Al and Cu–Al–Ni SMMs using the EAM. The alloys studied consist of elements with both FCC (for Cu, Al and Ni) and HCP (for Zn) structures. Since the functions expressed as cubic splines (Daw and Baskes 1984) are more flexible and we have succeeded in fitting experimental physical properties of Zn by appropriately selecting the spline knots, we make use of the original cubic spline functions in the present work, although there have been many analytical functional forms with some adjustable parameters proposed by Foiles *et al* (1986), Oh and Johnson (1988), Baskes *et al* (1989), Chen *et al* (1990), Adams and Foiles (1990) and Baskes (1992). The calculated results are then compared with the experimental data and are discussed in conjunction with the existing concept.

2. Embedded-atom method calculation

According to the EAM, the total energy for an arbitrary arrangement of nuclei can be written as

$$E_{\text{tot}} = \sum_i F_i(\rho_i) + \tfrac{1}{2}\sum_i \sum_{j \neq i} \varphi_{ij}(r) \tag{1}$$

where F_i is the embedding energy of the ith atom, ρ_i is the local electron density at the position of the ith atom provided by the other atoms of the system, and φ_{ij} is the short-range pair potential energy describing the core–core interaction. The pair potential φ_{ij} between atoms i and j was found to be equal to the geometrical mean of φ_{ii} and φ_{jj} (Daw and Baskes 1984). This is equivalent to expressing φ_{ij} in terms of the effective charges Z_i as

$$\varphi_{ij}(r) = \frac{Z_i(r)Z_j(r)}{r}. \tag{2}$$

To apply this method, the embedding function $F(\rho)$, the effective charge $Z(r)$ of every type of atom in the system concerned, and the electron densities ρ_i must be known. The electron densities ρ_i are calculated in this work according to Clementi and Roetti (1974). According to Daw and Baskes (1984), the functions F and Z can be taken as cubic splines in general and fitted empirically to reproduce experimental values of the lattice constant a_0, elastic constants C_{ij}, sublimation energy E_s and vacancy formation energy E_{1v}.

Table 1. Quantities used for determining the functions $F(\rho)$ and $Z(r)$ for Cu, Al, Ni and Zn.

		a_0 (Å)	c_0 (Å)	C_{11} (10^{11} Pa)	C_{12} (10^{11} Pa)	C_{44} (10^{11} Pa)	C_{13} (10^{11} Pa)	C_{33} (10^{11} Pa)	E_s (eV)	E_{1v} (eV)
Cu	Experimental	3.615		1.685	1.225	0.760			3.537	1.30
Cu	Fit	3.615		1.684	1.384	0.760			3.537	1.299
Zn	Experimental	2.6649	4.940	1.610	0.342	0.383	0.501	0.610	1.37	1.0
Zn	Fit	2.6518	5.4877	1.184	0.304	0.261	0.621	0.661	1.35	0.86
Al	Experimental	4.0496		1.082	0.613	0.285			3.36	0.66
Al	Fit ($3s^2$)	4.0774		0.888	0.687	0.301			3.358	0.652
Al	Fit ($3s^{1.7}$)	4.061		0.894	0.686	0.301			3.314	0.652
Ni	Experimental	3.52		2.465	1.473	1.247			4.45	1.40
Ni	Fit ($4s^{0.85}$)	3.523		2.399	1.497	1.265			4.456	1.398
Ni	Fit ($4s^1$)	3.523		2.399	1.497	1.265			4.456	1.398

We have determined the embedding functions $F(\rho)$ and effective charges $Z(r)$ for Cu, Al, Zn and Ni. The experimental physical quantities mentioned above are compared in table 1 with the fitted data. The atomic configurations used in the current calculations were $3d^{10}4s^1$ for Cu, $3d^{10}4s^2$ for Zn, $3s^23p^1$ for Al, and $3d^{9.15}4s^{0.85}$ for Ni, except in the case of the Cu–Al–Ni parent phase where the configurations of $3s^{1.7}3p^{1.3}$ for Al and $3d^94s^1$ for Ni were used. The fitted parameters for defining the functions $Z(r)$ and $F(\rho)$ for Cu, Al, Ni and Zn are listed in tables 2 and 3, respectively. The equilibrium densities $\bar{\rho}$, the positions r/a_0 and $\rho/\bar{\rho}$ of the spline knots and the function values at these knots are given.

In order to calculate the total energies for each given degree S of long-range order, the atomic configurations of the parent and $18R_1$ martensite phases must be known. A description of the atomic configurations of several martensites was given schematically by

Table 2. Fitted parameters for defining the functions $Z(r)$ and $F(\rho)$: spline knots r/a_0 and the function values of the effective charges.

Cu	r/a_0	0.00	0.43	0.65	0.71	0.85
Cu	$Z(r)$, $N_s = 1.0$	29.0	6.8705	0.3393	0.1431	0.0
Al	r/a_0	0.00	0.43	0.65	0.71	0.85
Al	$Z(r)$, $N_s = 2.0$	13.0	6.1288	0.3443	0.1242	0.0
	$N_s = 1.7$	13.0	3.8981	0.2563	0.1101	0.0
Ni	r/a_0	0.00	0.43	0.65	0.71	0.85
Ni	$Z(r)$, $N_s = 0.85$	28.0	6.4871	0.3499	0.1457	0.0
	$N_s = 1.0$	28.0	6.7523	0.3610	0.1479	0.0
Zn	r/a_0	0.00	0.48	0.81	1.00	1.75
Zn	$Z(r)$, $N_s = 2.0$	30.0	4.3635	0.4541	0.3573	0.0

Table 3. Fitted parameters for defining the functions $Z(r)$ and $F(\rho)$: spline knots $\rho/\bar{\rho}$, equilibrium densities $\bar{\rho}$ and the function values of the embedding functions $F(\rho)$.

Cu	$\rho/\bar{\rho}$	0.0	0.5	1.0	2.0	2.3
Cu	$F(\rho)$, $N_s = 1.0$, $\bar{\rho} = 41.7$ nm^{-3}	0.0	−2.8714	−4.2693	−2.9151	0.0
Al	$\rho/\bar{\rho}$	0.0	0.5	1.0	2.0	2.3
Al	$F(\rho)$, $N_s = 2.0$, $\bar{\rho} = 29.4$ nm^{-3}	0.0	−2.8145	−3.8527	−2.3404	0.0
	$N_s = 1.7$, $\bar{\rho} = 33.8$ nm^{-3}	0.0	−2.7246	−3.7059	−2.2213	0.0
Ni	$\rho/\bar{\rho}$	0.0	0.5	1.0	2.0	2.3
Ni	$F(\rho)$, $N_s = 0.85$, $\bar{\rho} = 28.6$ nm^{-3}	0.0	−3.6394	−5.2423	−3.4927	0.0
	$N_s = 1.0$, $\bar{\rho} = 33.5$ nm^{-3}	0.0	−3.6551	−5.2722	−3.5078	0.0
Zn	$\rho/\bar{\rho}$	0.0	0.49	1.2	2.0	2.7
Zn	$F(\rho)$, $N_s = 2.0$, $\bar{\rho} = 28.1$ nm^{-3}	0.0	−2.2790	−5.0975	−6.0	0.0

Wang *et al* (1987). By using the parameter x (Gui *et al* 1988), i.e. the component of the relative displacement of the neighbouring (001) martensite basal plane along the [100] martensite direction, and noting the stacking sequence of the $18R_1$ martensite (Delaey *et al* 1981), it is easy to write down all the coordinates of the atoms in the $18R_1$ martensite. The concrete atomic configuration depends on the degree S of long-range order. For the B2-type ordered parent (CsCl type) and 9R martensite phases, there are two sublattices. In the perfect B2-type order state ($S_{B2} = 1$), sublattice I is occupied by Cu atoms while sublattice II is occupied by Al, Zn (or Ni) and the remaining Cu atoms. In the A2-type disordered state ($S_{B2} = 0$) the occupations of the two sublattices are the same. Let C_{Cu}, C_{Zn} and C_{Al} be the atomic fractions of Cu, Zn and Al atoms, respectively, with $C_{Cu} + C_{Zn} + C_{Al} = 1$; then the fractions of each atom in the Cu–Zn–Al alloys on sublattices I and II are those listed in table 4. For Cu–Al–Ni alloys we need only substitute Zn by Ni.

Table 4. Atom occupation fractions in the B2-type ordered phases.

	Sublattice I	Sublattice II
Al	$(1 - S_{B2})C_{Al}$	$(1 + S_{B2})C_{Al}$
Zn	$(1 - S_{B2})C_{Zn}$	$(1 + S_{B2})C_{Zn}$
Cu	$1 - (1 - S_{B2})(C_{Al} + C_{Zn})$	$1 - (1 + S_{B2})(C_{Al} + C_{Zn})$

For the $D0_3$-type (or more accurately $L2_1$-type) ordered parent and $18R_1$ martensite phases, the above-mentioned sublattice II is divided further into two sublattices, i.e. sublattices 3 and 4. In the perfect $L2_1$-type order state ($S_{L2} = 1$), all Zn (or Ni) atoms lie on

sublattice 3 while Al atoms lie on sublattice 4. The ordering state with $S_{L2} = 0$ corresponds to that with $S_{B2} = 1$. Therefore we have the atom occupation fractions for the $L2_1$-type ordered Cu–Zn–Al alloys as listed in table 5.

Table 5. Atom occupation fractions in sublattices 3 and 4 of the $L2_1$-type ordered phases.

	Sublattice 3	Sublattice 4
Al	$(1 - S_{L2})2C_{Al}$	$(1 + S_{L2})2C_{Al}$
Zn	$(1 + S_{L2})2C_{Zn}$	$(1 - S_{L2})2C_{Zn}$
Cu	$2C_{Cu} - 1 + 2S_{L2}(C_{Al} - C_{Zn})$	$2C_{Cu} - 1 + 2S_{L2}(C_{Zn} - C_{Al})$

Table 6. Heat treatments of specimens.

	Cu–Zn–Al	Cu–Al–Ni
Directly quenched	Solid solution treated at 1073 K for 5 min; then quenched into ice-water directly	Solid solution treated at 1223 K for 5 min; then quenched into cold 10% NaOH solution
Step quenched	Solid solution treated at 1073 K for 5 min; then quenched into an oil bath at 433 K for 4 min; then quenched into cold water	Solid solution treated at 1223 K for 5 min; then quenched into an oil bath at 433 K for 4 min; then quenched into cold water

3. Experimental method

Several Cu–Zn–Al and Cu–Al–Ni alloys were prepared using raw materials of industrial purity. Plate specimens and filings enveloped in copper foils were subjected to direct quenching and step quenching. The heat treatment processes are listed in table 6. X-ray polycrystalline diffraction patterns were then taken by using an XD-3A (for lattice parameter determination) or D/max-rA rotating-anode x-ray diffractometer (for integrated intensity measurement). The method for determining the lattice parameters a, b, c and β from the x-ray diffraction pattern was described by Gui *et al* (1988), from which the bond angle φ in the martensite basal plane can be calculated as

$$\varphi = 2\tan^{-1}(b/a) \tag{3a}$$

for 9R and

$$\varphi = 2\tan^{-1}(b/2a) \tag{3b}$$

for $18R_1$ martensites, respectively. The method for measuring the degrees S of long-range order was described by Gui *et al* (1990) with a minor variation that the partial structure factor F_b for superreflections of the perfect B2-type ordered 9R martensite is expressed as

$$F_b = 2C_{Al}(f_{Cu} - f_{Al}) + 2C_{Zn}(f_{Cu} - f_{Zn}) \tag{4}$$

in accordance with table 4 and that for the perfect $L2_1$-type ordered $18R_1$ martensite should be expressed as

$$F_b = 4C_{Al}(f_{Cu} - f_{Al}) + 4C_{Zn}(f_{Zn} - f_{Cu}) \tag{5}$$

in accordance with table 5.

4. Results

4.1. Variation in the total energy with the lattice parameters

For each given degree of long-range order we calculated the variation in the energy of the parent phase with the lattice parameter for both Cu–Zn–Al and Cu–Al–Ni alloys. If we note that the edge length of the unit cell of the $L2_1$ and $D0_3$ ordered parent phases is double that of the B2 ordered parent phase, figure 1 shows a series of curves of the total energy against $2a_{B2}$ and a_{L2} of the $Cu_{70.8}Zn_{15.2}Al_{14.0}$ parent phase for different given degrees S_{B2} or S_{L2} of long-range order. It is clear that each curve for a given order degree possesses a minimum. The minimal energy E_{min} and corresponding lattice parameter a_{B2} (or a_{L2}) for a given order degree are taken as the theoretical total energy and lattice constant of the parent phase at a given order degree. Other Cu–Zn–Al and Cu–Al–Ni alloys show similar behaviours.

For the 9R and $18R_1$ martensites mentioned above, the total energy is a funciton of four lattice parameters a, b, c and β (or the parameter x) for each given order degree. In this case, there is still a minimum, and the minimal energy E_{min} and the corresponding lattice parameters a, b, c and β were calculated using the simplex optimization method.

4.2. Variation in the total energy and lattice parameters with the degree of long-range order

From figure 1 it is clear that lattice parameters $2a_{B2}$ and a_{L2}, i.e. the values corresponding to the minima of the curves, decrease with increase in the order degree, as demonstrated in figure 2. The variation is steeper on increase in S_{B2} than on increase in S_{L2}. Figure 2 demonstrates also the variation in the lattice parameters of the $Cu_{70.3}Al_{25.1}Ni_{4.6}$ parent phase with the order degree, which shows the same behaviour as the Cu–Zn–Al parent phase.

Figure 1 also shows that the minimal total energy E_{min} of the $Cu_{70.8}Zn_{15.2}Al_{14.0}$ parent phase decreases with increase in the order degree. This is demonstrated by the dashed line in figure 3. The $Cu_{70.3}Al_{25.1}Ni_{4.6}$ parent phase shows a similar behaviour (not shown).

Table 7 lists some of the calculated results for 9R and $18R_1$ $Cu_{70.8}Zn_{15.2}Al_{14.0}$ martensites, showing the variation in the minimal total energy E_{min} and corresponding lattice parameters a, b, c and β with the degree S of long-range order. Table 7 shows that an increase in both S_{B2} and S_{L2}, E_{min}, a and β decrease, b increases, and c remains nearly invariant. The variation in these parameters with the B2-type order degree S_{B2} for Cu–Al–Ni martensite is similar to that for Cu–Zn–Al martensite, while it demonstrates another variation with the $L2_1$-type order degree, as listed in table 8. Table 8 shows that, on increase in S_{L2}, E_{min} and b decrease, a and β increase, and c remains nearly invariant.

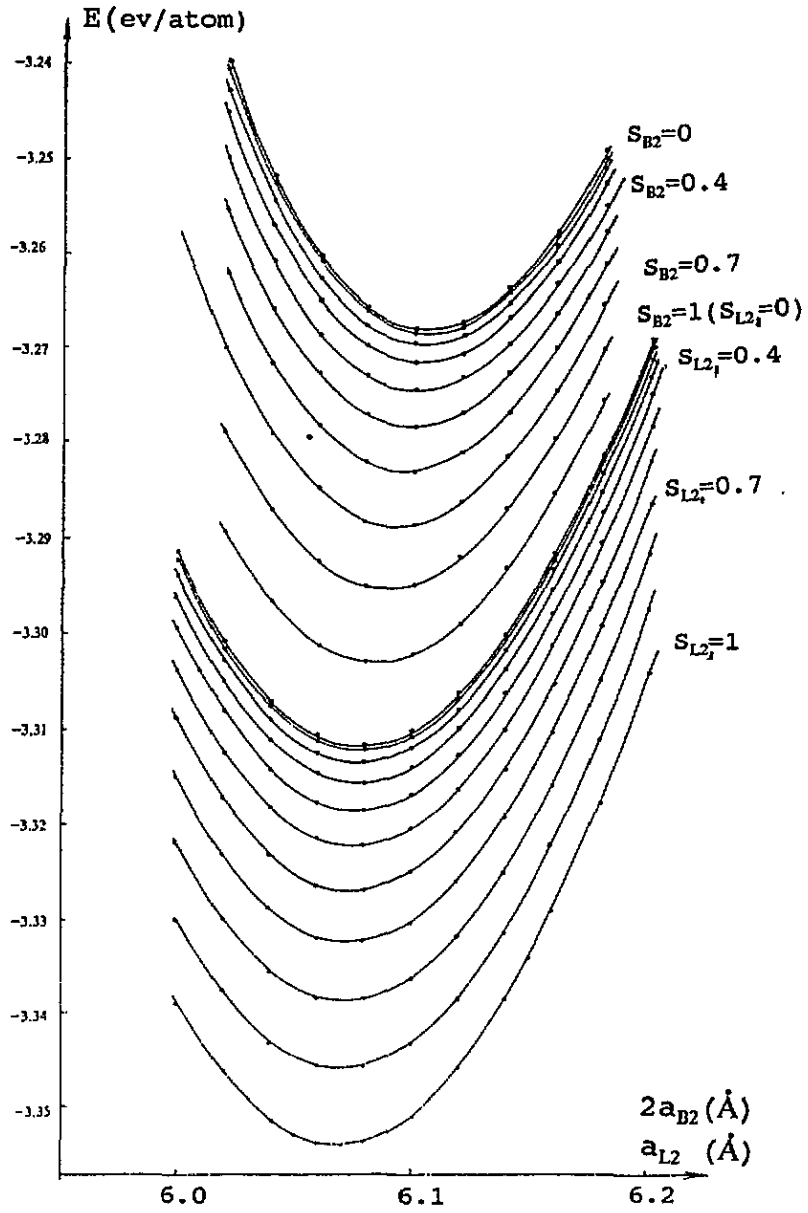

Figure 1. Curves of the total energy E against the lattice parameters $2a_{B2}$ and a_{L2} of the $Cu_{70.8}Zn_{15.2}Al_{14.0}$ parent phase for different given degrees S_{B2} and S_{L2} of long-range order.

The variation in the minimal total energy E_{min} of the 9R and $18R_1$ $Cu_{70.8}Zn_{15.2}Al_{14.0}$ martensites with the order degree S, as listed in table 7, is demonstrated in figure 3 (solid line).

Figure 3 shows that the total energy of both parent and martensite phases of this alloy is lowered when the order degree is increased. This explains the ordering tendency of this alloy at appropriate lower temperatures. Figure 3 shows also that

$$E_{B2} > E_{L2} > E_{9R} > E_{18R} \tag{6}$$

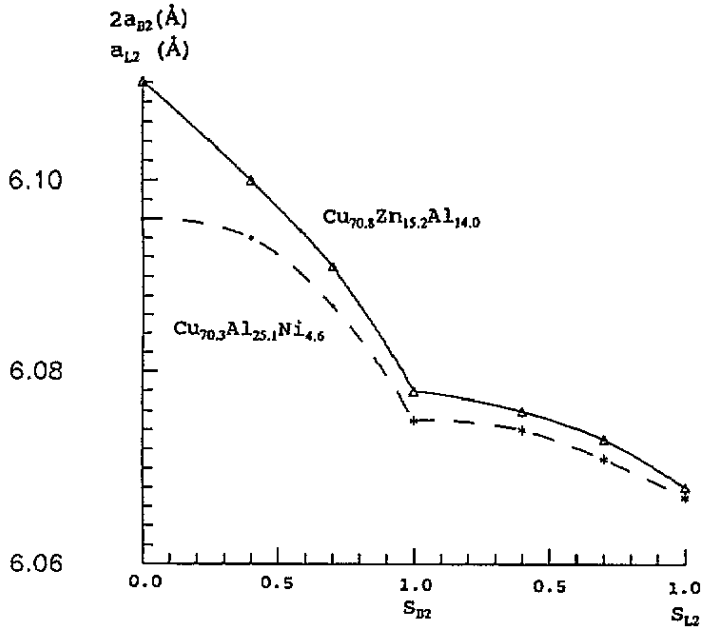

Figure 2. Variation in the lattice parameters $2a_{B2}$ and a_{L2} of the $Cu_{70.8}Zn_{15.2}Al_{14.0}$ (——) and $Cu_{70.3}Al_{25.1}Ni_{4.6}$ (– – –) parent phases as a function of the long-range degree S. Note that $S_{B2} = 1$ corresponds to $S_{L2} = 0$.

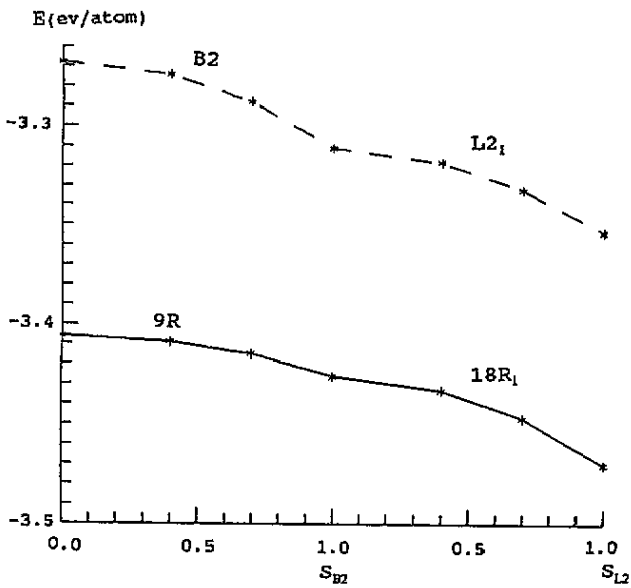

Figure 3. Variation in the minimal total energies E_{min} with the order degree S for the $Cu_{70.8}Zn_{15.2}Al_{14.0}$ alloy. Note that $S_{B2} = 1$ corresponds to $S_{L2} = 0$.

which implies the possibility of martensitic transformation at lower temperatures.

Table 7. Minimal total energies E_{min} and corresponding lattice parameters a, b, c and β of the 9R and 18R$_1$ $Cu_{70.8}Zn_{15.2}Al_{14.0}$ martensites at some given order degrees S.

	S	0.0	0.4	0.7	1.0
M9R	a (Å)	4.671	4.665	4.651	4.630
M9R	b (Å)	2.697	2.699	2.705	2.713
M9R	c (Å)	19.816	19.811	19.804	19.784
M9R	β (deg)	90.000	89.938	89.807	89.602
M9R	φ (deg)	60.000	60.113	60.360	60.731
M9R	E_{min} (eV/atom)	−3.406	−3.409	−3.415	−3.426
M18R$_1$	a (Å)	4.630	4.628	4.624	4.619
M18R$_1$	b (Å)	5.425	5.429	5.436	5.446
M18R$_1$	c (Å)	39.569	39.573	39.579	39.590
M18R$_1$	β (deg)	89.600	89.571	89.512	89.429
M18R$_1$	φ (deg)	60.731	60.785	60.890	61.043
M18R$_1$	E_{min} (eV/atom)	−3.426	−3.433	−3.447	−3.470

Table 8. Minimal total energies E_{min} and corresponding lattice parameters a, b, c and β of the 18R$_1$ $Cu_{70.3}Al_{25.1}Ni_{4.6}$ martensite at some given order degrees S_{L2}.

S	a (Å)	b (Å)	c (Å)	β (deg)	φ (deg)	E_{min} (eV/atom)
0.0	4.6736	5.4817	39.9724	89.5683	60.779	−3.5050
0.1	4.6698	5.4769	39.9611	89.5888	60.776	−3.5053
0.2	4.6829	5.4915	39.9740	89.6805	60.769	−3.5063
0.3	4.6729	5.4775	39.9506	89.5839	60.748	−3.5080
0.4	4.6726	5.4743	39.9413	89.5917	60.722	−3.5104
0.5	4.6724	5.4707	39.9380	89.5936	60.692	−3.5135
0.6	4.6904	5.4603	39.9573	89.7757	60.405	−3.5177
0.7	4.6932	5.4544	39.9493	89.8286	60.321	−3.5225
0.8	4.6971	5.4471	39.9439	89.8837	60.213	−3.5281
0.9	4.7008	5.4383	39.9245	89.9498	60.093	−3.5346
1.0	4.7010	5.4365	39.9280	89.9857	60.075	−3.5422

4.3. Variation in the bond angle φ in the basal plane of the martensite with the order degree

By using equation (3) the bond angles φ in the basal plane of the martensite were calculated from the lattice parameters a and b, some of which are listed in tables 7 and 8.

Figure 4 demonstrates the variation in the bond angle φ with the degree S of long-range order for several realistic and fictitious Cu-based alloys. It shows clearly that φ is equal to 60° corresponding to the regular hexagonal configuration of atoms when $S_{B2} = 0$ (A2-type disordered state). φ increases with increase in S_{B2} for all Cu-based alloys studied. For the $Cu_{69.6}Zn_{17.4}Al_{13.0}$ (curve 1), $Cu_{67.1}Zn_{24.0}Al_{8.9}$ (curve 2), $Cu_{70.8}Zn_{15.2}Al_{14.0}$ (curve 3) and $Cu_{69.5}Zn_{14.4}Al_{16.1}$ (curve 4) shape memory alloys, the bond angle φ increases with increasing $L2_1$-type order degree S_{L2}. On the contrary, for the $Cu_{68.4}Al_{27.8}Ni_{3.8}$ (curve 8) and $Cu_{70.3}Al_{25.1}Ni_{4.6}$ (curve 9) shape memory alloys, φ decreases towards 60° with increasing S_{L2}.

In order to understand the influence of the alloy composition on the φ versus S behaviour, we made some complementary calculations with less Zn content (curves 5 and 6) which show a nearly invariant φ angle when S_{L2} increases. The behaviour for Cu_3Al (curve 7) alloy is similar to those for Cu–Al–Ni alloys.

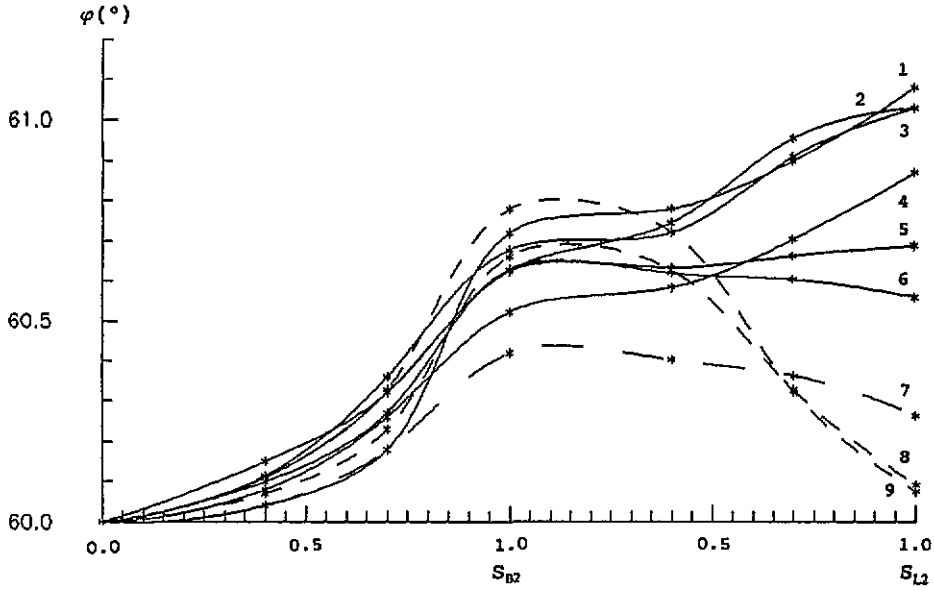

Figure 4. Variation in the bond angle φ with order degree S for several Cu-based alloys. Note that $S_{B2} = 1$ corresponds to $S_{L2} = 0$: curve 1, $Cu_{69.6}Zn_{17.4}Al_{13.0}$; curve 2, $Cu_{67.1}Zn_{24.0}Al_{8.9}$; curve 3, $Cu_{70.8}Zn_{15.2}Al_{14.0}$; curve 4, $Cu_{69.5}Zn_{14.4}Al_{16.1}$; curve 5, $Cu_{70}Zn_5Al_{25}$; curve 6, $Cu_{70}Zn_2Al_{28}$; curve 7, Cu_3Al; curve 8, $Cu_{68.4}Al_{27.8}Ni_{3.8}$; curve 9, $Cu_{70.3}Al_{25.1}Ni_{4.6}$.

4.4. Comparison with experimental results

Figure 5 shows portions of x-ray diffraction patterns from the plate specimens of the $Cu_{69.5}Zn_{14.4}Al_{16.1}$ shape memory alloy which could not be regarded as isotropic polycrystalline owing to their large grain size and the possible rolling texture. It is clearly seen from these patterns that the line pairs $\bar{1}22$–202, $1\,2\,\bar{1}0$–$\bar{2}\,0\,10$ and 040–320 have less separation, corresponding to a smaller φ angle, for the directly quenched specimen (figure 5(*a*)) than the specimen step quenched at 433 K (figure 5(*b*)). The lattice parameters a, b, c and β of the directly quenched and step-quenched the method described by Gui *et al* (1988) and the experimental bond angles φ were then obtained by equation (3*b*). These experimental values are listed in table 9.

Table 9. Experimental separation values $2\theta_{hkl} - 2\theta_{h'k'l'}$, lattice parameters a, b, c and β and bond angles φ of M18R$_1$ martensite in $Cu_{69.5}Zn_{14.4}Al_{16.1}$ and $Cu_{68.7}Al_{27.8}Ni_{3.5}$ alloys.

	$Cu_{69.5}Zn_{14.4}Al_{16.1}$		$Cu_{68.7}Al_{27.8}Ni_{3.5}$	
	Directly quenched	Step quenched	Directly quenched	Step quenched
$2\theta_{202} - 2\theta_{\bar{1}22}$ (deg)	0.90	1.52	1.47	1.35
$2\theta_{2\,1\,\bar{1}0} - 2\theta_{1\,2\,\bar{1}0}$ (deg)	1.80	2.15	2.22	2.20
$2\theta_{320} - 2\theta_{040}$ (deg)	2.20	2.85	3.33	3.00
a (Å)	4.438	4.422	4.389	4.393
b (Å)	5.319	5.334	5.347	5.340
c (Å)	38.21	38.29	38.02	37.88
β (deg)	88.46	88.72	88.62	89.14
φ (deg)	61.86	62.19	62.69	62.58

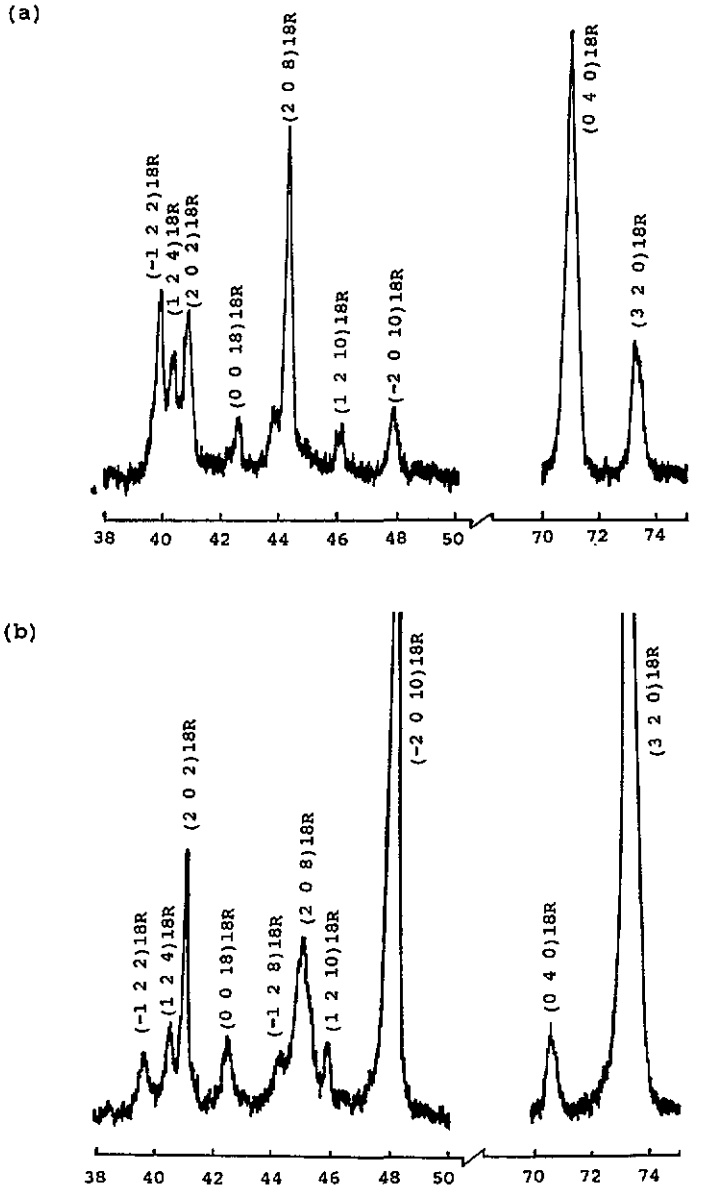

Figure 5. X-ray diffraction patterns of plate specimens of the $Cu_{69.5}Zn_{14.4}Al_{16.1}$ shape memory alloy: (*a*) directly quenched; (*b*) step quenched.

Figure 6 shows portions of x-ray diffraction patterns from plate specimens of the $Cu_{68.7}Al_{27.8}Ni_{3.5}$ shape memory alloy. In contrast with the Cu–Zn–Al alloys, here the line pairs have a larger separation, indicating a larger φ angle for the directly quenched specimen (figure 6(*a*)) than for the step-quenched specimen (figure 6(*b*)). The related experimental values are also listed in table 9.

Table 10 lists the experimental bond angles φ and order degrees S_{L2} of $18R_1$ martensite in several Cu-based alloys subjected to direct and step quenching, respectively.

According to Rapacioli and Ahlers (1977) and Singh *et al* (1978), the critical ordering

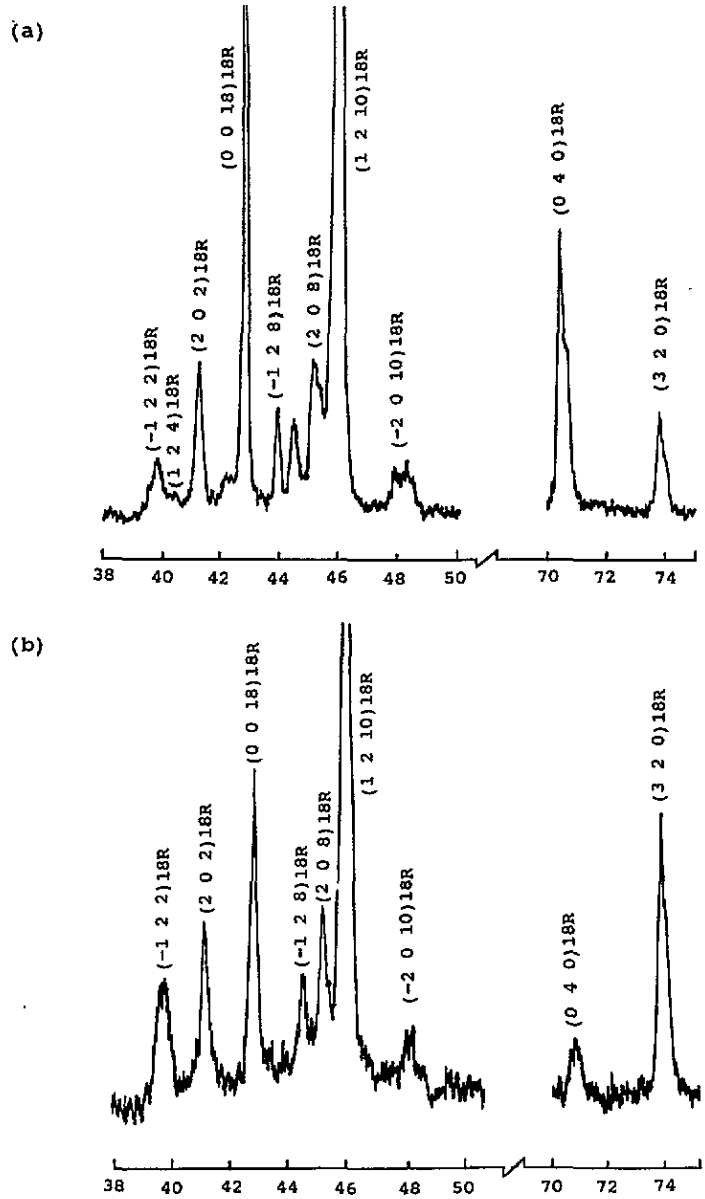

Figure 6. X-ray diffraction patterns of plate specimens of the $Cu_{68.7}Al_{27.8}Ni_{3.5}$ shape memory alloy: (*a*) directly quenched; (*b*) step quenched.

temperatures for the Cu–Zn–Al alloys studied are nearly $T_{B2} = 770$ K and $T_{L2} = 660$ K, much higher than the holding temperature during step quenching. Therefore, the order degrees of the step quenched specimens should be higher than those of the directly quenched specimens. This is confirmed by the measured S_{L2} values listed in table 10. Therefore, table 10 indicates that, when the order degree S_{L2} increases (from the directly quenched martensite to the step quenched martensite), the bond angle φ increases for the Cu–Zn–Al alloys and decreases for the Cu–Al–Ni alloys, in qualitative agreement with the theoretical results mentioned in section 4.3.

Table 10. Experimental bond angles φ and order degrees S_{L2} of M18R$_1$ martensite in several Cu-based alloys subjected to different heat treatments.

	Directly quenched		Step quenched	
Composition (at.%)	φ (deg)	S_{L2}	φ (deg)	S_{L2}
$Cu_{69.6}Zn_{17.4}Al_{13.0}$	61.32	0.73 ± 0.04	61.69	0.80 ± 0.04
$Cu_{70.8}Zn_{15.2}Al_{14.0}$	61.15	0.72 ± 0.04	61.33	0.76 ± 0.04
$Cu_{70.2}Zn_{17.7}Al_{12.1}$	61.31		61.71	
$Cu_{70.2}Zn_{15.4}Al_{14.4}$	61.31		61.67	
$Cu_{69.5}Zn_{14.4}Al_{16.1}$	61.86		62.19	
$Cu_{70.3}Al_{25.1}Ni_{4.6}$	62.17		61.42	
$Cu_{68.7}Al_{27.8}Ni_{3.5}$	62.69		62.58	

5. Discussion

So far as the present authors know, this paper is the first application of the EAM to shape memory alloys. The EAM calculation confirmed several experimental results, such as the ordering tendency of these alloys, the possibility of martensitic transformation in these alloys, and the dependence of the atomic configuration in the basal plane of the 9R martensite on the order degree. The latter fact was explained by the hard-sphere model in the past (Tadaki *et al* 1975, Delaey *et al* 1981). However, in contrast with the previous statement that the B2-type ordering is liable to produce more severe deviation from the regular hexagonal configuration of the atoms than A2 and $D0_3$-type ordering, the EAM results indicates that $L2_1$-type ordered ($S_{L2} = 1$) Cu–Zn–Al 18R$_1$ martensite possesses a larger bond angle φ than $B2$-type ordered ($S_{B2} = 1$, $S_{L2} = 0$) martensite, and the relation between φ and S_{L2} is composition dependent. As mentioned in section 4.4, this calculated result is in qualitative agreement with the experimental φ-values measured from specimens of different order degrees S_{L2}.

By comparing the theoretical angles φ shown in figure 4 with the experimental values listed in table 10, we find that they are not in quantitative agreement. The experimental angles φ are larger than the calculated values for any given order degree S_{L2} of any alloy studied. This discrepancy may be explained as follows.

The martensite transformation induces strong local strains which prevent transformation to the stable martensite structure as calculated by the EAM. Instead an intermediate martensite structure results with φ lying between 70.5° (the value for the parent phase) and the value shown in figure 4.

In the present paper, we explained the possibility of martensitic transformation at lower temperatures by comparing the total energy of the parent phase with that of the martensite; see equation (6) in section 4.2 of this paper. Willaime and Massobrio (1989, 1991) studied the kinetics of the BCC-to-HCP phase transformation in zirconium by using the EAM. They found that the transverse phonon with a wavevector along the $[110]_{BCC}$ direction and displacements along the $[1\bar{1}0]_{BCC}$ direction is unstable. This calculation confirms the Burgers mechanism of the BCC-to-HCP phase transition. This mechanism was accepted by some workers as explaining the martensitic transformation in some shape memory alloys (see, e.g., Nishiyama and Kajiwara (1963)). It may be interesting to apply the EAM to calculate the phonon characteristics of the parent and martensite phases in Cu-based SMMs in order to discuss the possible kinetics of the martensitic transformation.

Ceder *et al* (1989) calculated the total Helmholtz free energy of different long-period superstructure (LPS) phases by means of the Gorsky–Bragg–Williams approximation in the axial next-nearest-neighbour Ising model and then discussed the relative stability of different

LPS phases. While this calculation considered the contribution from entropy, our EAM study concerned only the ground-state properties and hence can only by used to discuss the phase stability at lower temperatures. Therefore, the Ising model, as a phenomenological approach, may be a useful complement to the atomistic calculation by means of EAM for studying the ordered structures in SMMs.

Acknowledgment

This project was supported by the National Natural Science Foundation of China.

References

Adams J B and Foiles S M 1990 *Phys. Rev.* B **41** 3316
Ahlers M 1974 *Scr. Metall.* **8** 213
Baskes M I 1992 *Phys. Rev.* B **46** 2727
Baskes M I, Nelson J S and Wright A F 1989 *Phys. Rev.* B **40** 6085
Ceder G, De Graef M, Delaey L, Kulik J and de Fontaine D 1989 *Phys. Rev.* B **39** 381
Chen S P, Voter A F, Albers R C, Boring A M and Hay P J 1990 *J. Mater. Res.* **5** 955
Clementi E and Roetti C 1974 *At. Data Nucl. Data Tables* **14** Nos 3 and 4
Daw M S and Baskes M I 1984 *Phys. Rev.* B **29** 6443
Delaey L 1967 *Z. Metallk.* **58** 388
Delaey L, Chandrasekaran M, Andrade M and Van Humbeeck J 1981 *Proc. Int. Conf. on Solid–Solid Phase Transformations* ed H I Aaronson, D E Lauphlin, R E Sekerka and C M Wayman (Pittsburgh, PA: Metallurgical Society of AIME) p 1429
Delaey L, Suzuki T and Van Humbeeck J 1984 *Scr. Metall.* **18** 899
Ercolessi F , Tosatti E and Parrinello M 1986 *Surf. Sci.* **177** 314
Finnis M W and Sinclair J E 1984 *Phil. Mag.* A **50** 45
Foiles S M, Baskes M I and Daw M S 1986 *Phys. Rev.* B **33** 7983
Gui J, Luo C, Zhang H, Hu W and Wang R 1990 *J. Mater. Sci.* **25** 1675
Gui J, Wang R and Zhao Y 1988 *J. Appl. Crystallogr.* **21** 340
Liu D, Wang R and Ye Y 1991 *Phys. Rev.* B **43** 4648
Nie X, Wang R and Ye Y 1988 *Phys. Status Solidi* b **177** 261
Ning T, Yu Q and Ye Y 1988 *Surf. Sci.* **206** L857
Nishiyama Z and Kajiwara S 1963 *Japan. J. Appl. Phys.* **2** 478
Oh D J and Johnson R A 1988 *J. Mater. Res.* **3** 471
Rapacioli R and Ahlers M 1977 *Scr. Metall.* **11** 1147
Scarsbrook G, Cook J M and Stobbs W M 1982 *J. Physique* **43** C4 703
Singh S C, Murakami Y and Delaey L 1978 *Scr. Metall.* **12** 435
Smith J R and Banerjea A 1987 *Phys. Rev. Lett.* **59** 2451
Tadaki T, Tokoro M and Shimizu K 1975 *Trans. Japan Inst. Met.* **16** 287
Wang R, Zhao Y and Gui J 1987 *J. Electron Microsc. Technique* **7** 293
Willaime F and Massobrio C 1989 *Phys. Rev. Lett.* **63** 2244
—— 1991 *Phys. Rev.* B **43** 11 653